UDC 535.33:
533.6

TECHNICAL REPORT OF NATIONAL AEROSPACE LABORATORY

TR-351T

Time-Resolved Spectroscopic Measurements Behind Incident and Reflected Shock Waves in Air and Xenon

Takashi YOSHINAGA

December 1973

NATIONAL AEROSPACE LABORATORY

CHŌFU, TOKYO, JAPAN

List of NAL Technical Reports

TR–330T On the Linear Theory of Thin Elastic Shells	Tatsuzo KOGA & Susumu TODA	Jul. 1973
TR–331 A Non-linear Hydrodynamic Stability Theory with Numerical Calculations—Part 1 A Power Series Method for the Numerical Treatment of the Orr-Sommerfeld Equation—	Nobutake ITO	Jul. 1973
TR-332 A Non-linear Hydrodynamic Stability Theory with Numerical Calculations—Part 2 Theoretical Analysis and the Numerical Results for Plane Poiseuille Flow—	Nobutake ITO	Jul. 1973
TR–333 A Non-linear Hydrodynamic Stability Theory with Numerical Calculations—Part 3 Numerical Results for the Flat Plate Boundary Layer—	Nobutake ITO	Jul. 1973
TR–334 Distortions of Sonic Boom Preasure Signature by Sound and Turbulence Interaction	Nagamasa KONO	Aug. 1973
TR–335 Design and Development of the Gust Wind Tunnel at the National Aerospace Laboratory	Kenichi HIROSUE, Kiyomi KITAMURA, Yoshitaka MURAKAMI & Shigemi SHINDO	Sept. 1973
TR–336 Strain Analysis by the Moire Analyzer Method	Yoshio AOKI	Sept. 1973
TR–337 An Analysis of the Equations of Motion for Rotary-drive Vibratory-output Gyros	Hiroshi YAMADA	Oct. 1973
TR–338 Analysis on a Passive Magnetic Suspension System with an Eight Pole Stator for Floated Inertial Sensors	Minoru TAKIZAWA, Masao OTSUKI & Takao SUZUKI	Sept. 1973
TR–339 A Test of a Swept-back Wing Model Conducted in the NAL $2^m \times 2^m$ Transonic Wind Tunnel	Masao EBIHARA, Shinsaku SEGAWA & Tokio OKONOGI	Oct. 1973
TR–340 Study of a Radial-exiting Hysteresis Gyro Motor	Hiroshi YAMADA	Nov. 1973
TR–341 Low-Pressure Detlagration Limit of Controllable Solid Rocket Propellants	Tomifumi GODAI, Morio SHIMIZU, Katsuya ITO, Hisao NISHIMURA, Toshiharu TANEMURA & Tsutomu FUJIWARA	Oct. 1973
TR–342 Study of a Rotary-drive Vibratory-output Accelerometer	Hiroshi YAMADA	Dec. 1973
TR–343 Path and Induced Field of a Jet Exhausting at a Large Angle into a Uniform Cross Flow	Hiroshi ENDO, Naoaki KUWANO, Teruomi NAKAYA, Nobuhiro TODA & Shigeru HIDAWA	Oct. 1973
TR–344 Active Nutation Control of a Spinning Axi-Symmetric Satellite Using a Gas Jet	Chikara MURAKAMI & Atsushi NAKAJIMA	Oct. 1973
TR–345 An Experimental Investigation of Flat-Plate Helical Inducers for Rocket Pumps	Kenjiro KAMIJO & Akio SUZUKI	Oct. 1973
TR–346 An Observation on Spanwise Distribution of Vertical Atmospheric Turbulence	Koichi ONO, Tokuo SOTOZAKI, Kazuyuki TAKEUCHI & Kosaburo YAMANE	Oct. 1973
TR–347 Off-design-point Performances of Multi-spool Turbo Fan Engines	Mitsuo MORITA & Shizuo SEKINE	Nov. 1973

Time-Resolved Spectroscopic Measurements Behind Incident and Reflected Shock Waves in Air and Xenon*

By Takashi YOSHINAGA**

要　約

宇宙間飛行する飛行体が他の惑星の大気に突入する場合，あるいは地球大気に再突入する場合，ふく射による飛行体への加熱は対流によるものより大きくなる。衝撃波からのふく射加熱の基礎的な知識を得るため，アーク加熱型衝撃波管を使って，原子量の大きい Xenon 気体と地球大気をシミュレートする人工空気を試料気体として，入射衝撃波および反射衝撃波からのスペクトルの時間的変化を調べた。初期圧は 1 torr と 0.1 torr の二種類で，衝撃波速度は 5～10 km であった。スペクトルの観測にはアブコ型回転ドラム付スペクトログラフを使用した。

ABSTRACT

Time-resolved spectra have been obtained behind incident and reflected shock waves in air and xenon at initial pressures of 0.1 and 1.0 torr using a rotating drum spectrograph and the OSU (The Ohio State University) arc-driven shock tube. These spectra were used to determine the qualitative nature of the flow as well as for making estimates of the available test time.

The $(n+1, n)$ and (n, n) band spectra of N_2^+ (1st negative) were observed in the test gas behind incident shock waves in air at $p_1=1.0$ torr and $U_S=9$–10 km/sec. Behind reflected shock waves in air, the continuum of spectra appeared to cover almost the entire wavelength of 2,500–7,000 Å for the shock-heated test gas.

For xenon, the spectra for the incident shock wave cases for $p_1=0.1$ torr show an interesting structure in which two intensely bright regions are witnessed in the time direction.

The spectra obtained behind reflected shock waves in xenon were also dominated by continuum radiation but included strong absorption spectra due to FeI and FeII from the moment the reflected shock passed and on.

1. INTRODUCTION

The study of radiative gasdynamics was first initiated by astronomers attempting to explain the observed nature of stars, the sun, and comets. Recently, the physics of high temperature gases has become increasingly important in other problems such as the propagation of energy from the center of nuclear explosion to the air surrounding it, in which the coupling of radiation and the blast wave itself exists, the containment of a plasma in a closed vessel at nuclear fusion conditions, and the thermal protection of re-entry vehicles.

Entry into the atmospheres of earth and other planets such as Venus, Mars, and Jupiter in the future may involve entry velocities ranging from 15 to 50 km/sec. The problems to be encountered at these speeds require a deeper understanding of high temperature phenomena in the hypersonic flow field around the vehicles, since the characteristics of these flow fields will differ from those associated with lower entry velocities.

In the high temperature flow fields associated with the higher vehicle velocities, radiation from the shock heated gas region is a dominant

* Received September 14, 1973

** First Aerodynamics Division

energy transfer mechanism. Because of the energy loss due to the radiation transferred upstream, the local gas temperature in the region behind the bow shock will differ from the temperature predicted by the equilibrium normal shock wave relations. The radiative transfer changes the flow field itself and its determination now requires calculations using the fundamental equations with radiation effects included.

In order to investigate these phenomena, shock tubes have been utilized and have proven to be a very powerful research tool. Using xenon as a driven gas, Golobic[1] carried out temperature measurements behind incident shock waves employing the two-line intensity ratio technique. This method necessarily was based on the use of fundamental atomic properties such as transition probabilities and line broadening properties. Bader[2] measured temperature at the same flow conditions utilizing the brightness temperature technique. This method does not use any fundamental atomic properties. In both methods, the selection of strongly radiating lines in the shock heated gas is important, and this was at least a part of the motivation behind this study.

The specific purpose of this research was first to determine the major radiators behind shock waves in xenon and air produced in an arc-heated shock tube and second to qualitatively determine the time resolved flow structure after the shock front.

The time-integrated spectra obtained by Golobic by exposing the spectrograph for the entire duration of a shock tube test does not allow one to distinguish between the radiation emitted by the test gas and that by the driver gas or contamination. It is also impossible to assess the time-dependent variation of the spectra.

The present experiments were carried out using both incident and reflected shock waves. In the case of the incident shock experiments, the downstream driven pressure was 1.0 torr for air and 0.1 and 1.0 torr for xenon. The incident shock velocity was about 10 km/sec in the case of air, and it ranged from 3 to 9 km/sec in the case of xenon. In the case of the reflected shock experiments, the downstream driven pressure was 1.0 torr for both air and xenon. The incident shock velocity ranged from 7 to 10 for air and was about 6 km/sec for xenon.

In the next section, the radiation properties of shock-heated gases will be reviewed with particular emphasis being placed on the radiative characteristics of xenon and air. This will be followed in Section III by a discussion of the instrumentation used in this study and in Section IV by a presentation and discussion of the experimental results obtained.

2. RADIATION IN AIR AND XENON

Properties of the Shock-Heated Gases

From one dimensional theory, the velocity of a shock wave in a shock tube is predicted to be a function of the pressure ratio across the diaphragm just before rupture of the diaphragm and the speeds of sound and specific heat ratios for the driver and driven gases, i.e.

$$\frac{p_4}{p_1}=\frac{2\gamma_1 M_1^2-(\gamma_1-1)}{\gamma_1+1}\times\left\{1-\frac{\gamma_4-1}{\gamma_1+1}\frac{a_1}{a_4}\left(M_1-\frac{1}{M_1}\right)\right\}^{-\left(\frac{2\gamma_4}{\gamma_4-1}\right)}$$

$$\frac{p_4}{p_1}\to\infty,\quad \left\{1-\frac{\gamma_4-1}{\gamma_1+1}\frac{a_1}{a_4}\left(M_1-\frac{1}{M_1}\right)\right\}\to 0$$

$$M_1\to\frac{\gamma_1+1}{\gamma_4-1}\frac{a_4}{a_1}$$

$$\therefore\quad V_1\to\frac{\gamma_1+1}{\gamma_4-1}a_4$$

As may be seen above, in the limiting case where the pressure ratio p_4/p_1 is infinite, the velocity of the shock wave depends on the speed of sound in driver gas, so that the maximum velocity of the shock wave obtainable is weakly dependent on the kind of gases used in the driven section of the shock tube. However, the conditions behind the shock wave such as temperature, pressure and density are functions of shock Mach number, and the speed of sound and the initial conditions in the driven gas. Since the speed of sound is inversely proportional to the square root of the molecular weight of the gas, for a given shock velocity the shock Mach number of a gas with a higher molecular weight will be higher than that for a gas with a lower molecular weight.

The Mach number difference for different gases at the same temperature and for the same shock wave velocity is calculated using the inverse ratio of the molecular weight ratio for the respective gases. Thus, the ratio of shock Mach numbers for xenon and air is 1.95, and for a 10 km/sec shock velocity, the shock Mach number in xenon is 55, while for air the shock Mach number is only 28.

Although the state behind a shock is often in non-equilibrium, the equilibrium conditions behind a shock wave obtained from the Ran-

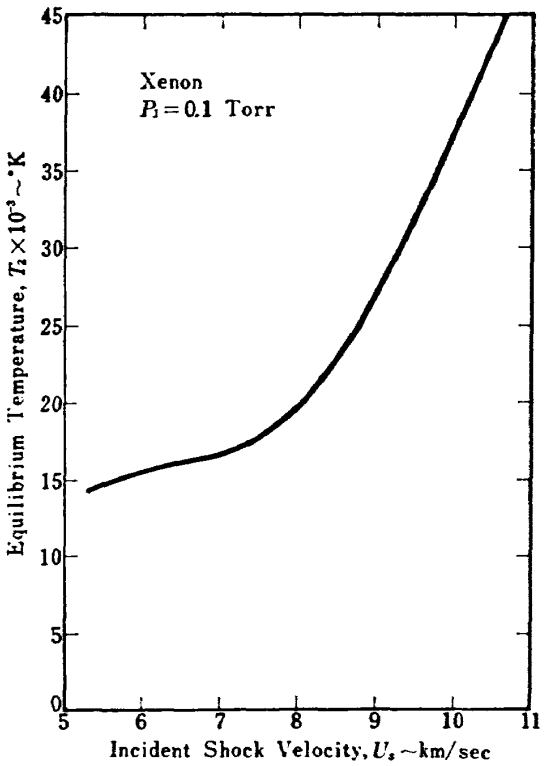

Figure 1. Equilibrium Temperature Behind Incident Shock Wave in Xenon as Calculated by Crawford (Ref. 3)

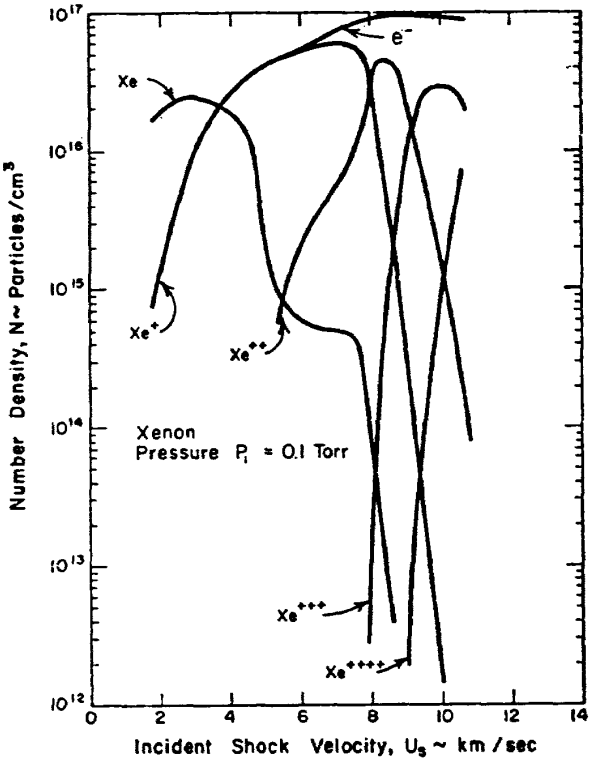

Figure 2. Equilibrium Number Densities Behind Incident Shock Wave in Xenon as Calculated by Crawford (Ref. 3), p_1=0.1 torr.

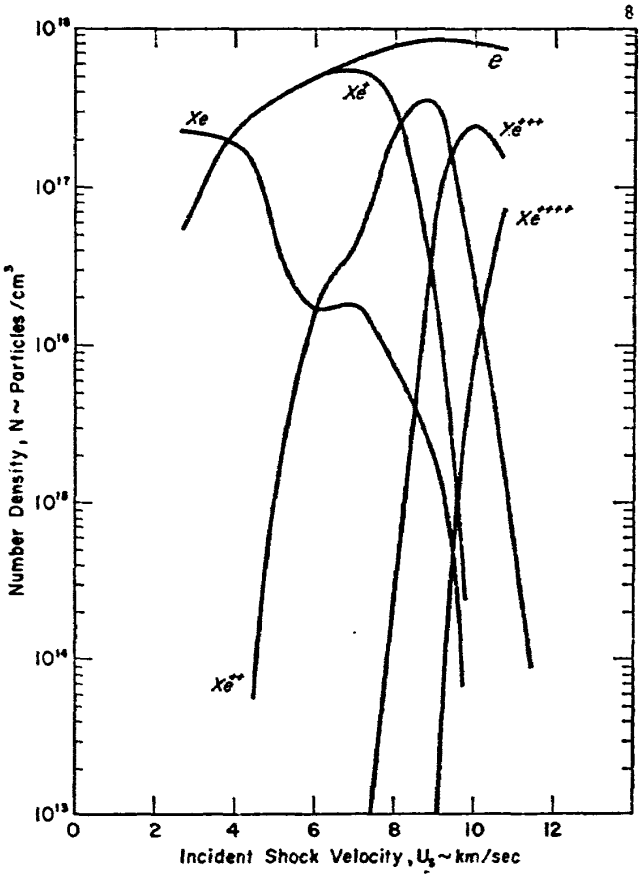

Figure 3. Equilibrium Number Densities Behind Incident Shock Wave in Xenon as Calculated by Crawford (Ref. 3), p_1=1.0 torr.

kine-Hugoniot relations are representative and may be used to infer the approximate conditions behind strong shock waves produced in shock tubes. Crawford[3] calculated the gas conditions behind incident and reflected shock wave in xenon. These predictions of the equilibrium temperature behind incident shock waves with an upstream pressure of 0.1 torr and an upstream temperature of 300°K are shown in Figure 1. At a shock velocity of 10 km/sec the post-shock equilibrium temperature in xenon is 40,000°K and is about four times greater than that in air. In Figures 2 and 3 the number density of each species of shock-heated xenon is presented as a function of velocity for driven pressures of 0.1 and 1.0 torr. This shows that at a pressure of 0.1 torr first ionization begins at a shock velocity of approximately 2 km/sec and becomes a maximum at a shock velocity of 5.5 km/sec. At this velocity most of the Xe atoms have ionized into Xe^+, and the second ionization of xenon begins. When the second ionization becomes maximum at the shock velocity of 8.5 km/sec, the singly ionized xenon has disappeared and third ionization is beginning. At

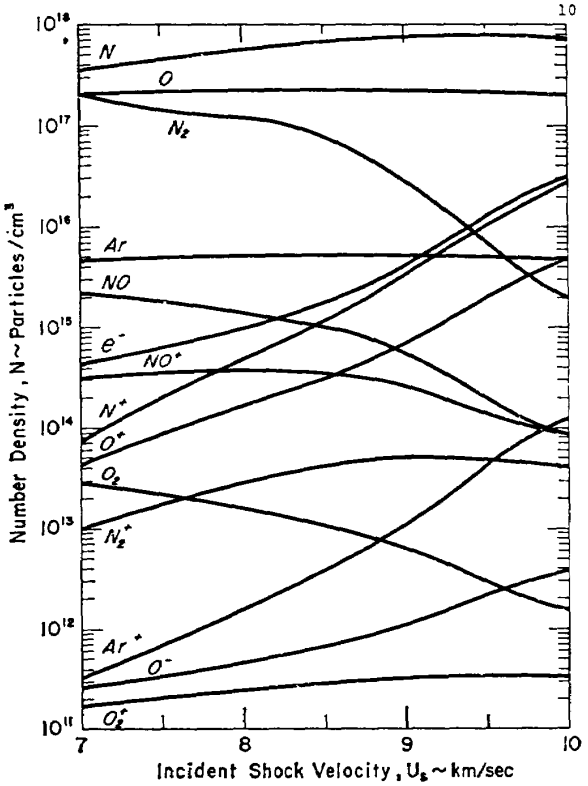

Figure 4. Equilibrium Number Densities Behind Incident Shock Wave in Air as Calculated by Menard and Horton (Ref. 4), p_1=1.0 torr

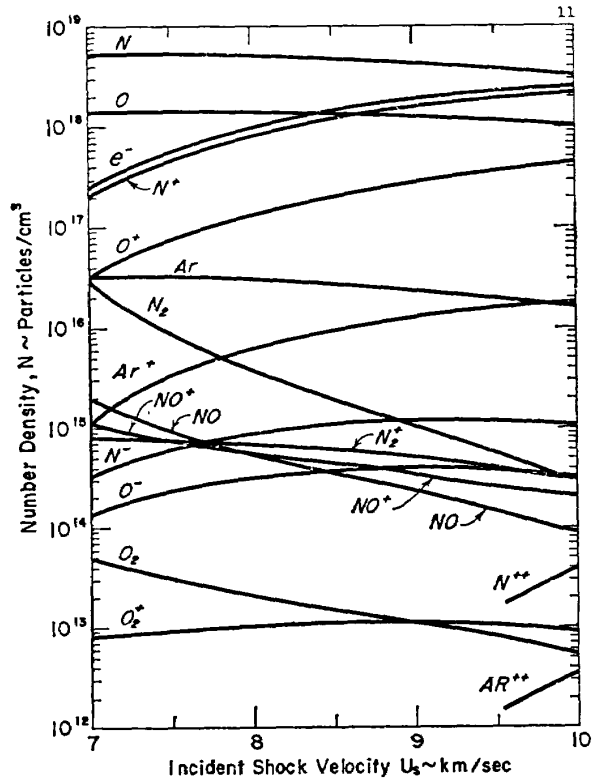

Figure 5. Equilibrium Number Densities Behind Reflected Shock Wave in Air as Calculated by Menard and Horton (Ref. 4), p_1=1.0 torr.

shock velocities in excess of 10 km/sec, fourth ionization occurs.

Similar calculations have been carried out by Menard and Horton[4] for incident and reflected shock waves in air. Their results for an initial pressure of 1.0 torr and an initial temperature of 300°K are shown in Figures 4 and 5.

The Nature of the Spectra

It is useful to explain here the general nature of spectra before we discuss the observed spectra from the present experiments in air and xenon. I will not attempt to refer to any detail of the theory of spectra. Gaydon and Hurle[5] have devoted an introductory chapter to a non-mathematical discussion of spectra in connection with flame spectroscopy and have given a somewhat more complete treatment of diatomic molecular spectra. A complete discussion of spectroscopic theory is given in the books by Herzberg[6,7], the recent book by Penner[8], and the book by Zel'dovich[9] where the fundamental physical aspects of radiation mechanisms are discussed. Following Gaydon and Hurle the general nature of spectra emitted by heated gases is here summarized.

An enclosed gas in complete equilibrium will emit a continuous spectrum similar to that of black body at the gas temperature, with its intensity and wavelength distribution defined by the Plank radiation law. In practice a gas which is unenclosed or enclosed by cooler walls will emit more radiation than it absorbs; under such conditions discrete spectra consisting of lines, bands and regions of continuum are observed.

The allowed electronic transitions in an atom accompanying the emission of light are subdivided into three types. These are:

(1) Bound-bound (discrete) transitions—

This transition yields line spectra. Line spectra are due to electronic transitions in free atoms, i.e. due to a change of 'orbit' of one or more electrons from one quantized energy state to another energy state.

(2) Free-bound transitions—

This transition yields continuous spectra. This process occurs when an electron passes close to a particle and is captured, releasing a photon.

In the case of xenon

$$Xe^+ + e^- \rightarrow Xe + h\nu$$
$$Xe^{++} + e^- \rightarrow Xe^+ + h\nu$$

(3) Free-free transitions—

This transition yields continuous spectra. This process is called Bremsstrahlung and oc-

curs when the passing electron is not captured but is decelerated with the release of a photon.

In the case of Xenon

$$Xe^+ + e^- \rightarrow Xe^+ + e^- + h\nu$$

Similar transitions are also expected when a diatomic gas is heated to high temperatures and the molecule decomposes into atoms.

The energy transitions in molecules are much more complicated.

Corresponding to each of the atomic transitions, the transitions for a molecule are:

(1) Bound-bound transitions—

The band spectra, in the visible and ultra violet regions, are due to the electronic transitions in molecules, but in these cases the electronic transition is accompanied by simultaneous changes in the internal vibrational and rotational energies of the molecules, so that each electronic transition is broken up into a number of bands, due to the change of vibrational energy, and each band is broken up into a large number of lines due to the changes in rotational energy. Band spectra in the near infrared may be due to the change of vibrational and rotational energy alone, without an accompanying electronic transition, and bands in the far infrared are due to the changes of rotational energy only.

(2) Free-bound transitions—

The important transition here is recombination of free electrons and ions.

(3) Free-free transitions (Bremsstrahlung)—

These two transitions (2) and (3) give the continuous spectra. There are also other mechanisms which cause the continuous spectra. One of them is emission due to the chemical reaction. However, in high temperature shock-heated gases, the ion recombination processes are responsible for most of the continuous emission. When the density is low, its intensity is proportional to the product of the electron concentration and the positive ion concentration (thus, to the square of the degree of ionization) and inversely proportional to the square root of the absolute temperature. The rapid increase in ionization with temperature is normally dominant, causing the continuum to strengthen very rapidly with temperature.

Spectra of Xenon and Air

Because of the low specific heat capacity of the higher molecular weight monatomic inert gases, it is possible to reach very high temperatures by shock heating and conditions of strong radiative emission are readily obtained. It is because of this that xenon has been of interest as a test gas. Air on the other hand is of obvious interest because of motivation provided by the problems of atmospheric entry, and it is these two gases, xenon and air, that have been included in this study.

In Figures 2 and 3, the equilibrium composition for xenon was presented as a function of shock velocity for a driven pressure of 0.1 torr and 1.0 torr as calculated by Crawford[9]. Although the actual condition behind a shock wave in xenon may be in nonequilibrium, these figures give an indication of the type of conditions attainable. Golobic[1] presented in his dissertation time integrated spectra obtained behind incident shock waves in xenon. These spectra indicate that XeII and XeIII are the dominant radiators. Although there were more XeII lines, the XeIII lines that appeared were relatively as bright as the XeII lines. Iron and C_2 were the contaminants present as emission spectra. No neutral xenon lines appeared in the spectra.

Roth[10] and Gloersen[11] found that the continuum did not have uniform intensity for xenon, falling by about 60 percent between 5,500 and 4,950 Å and that its strength was not proportional to the square of the expected ion concentration. Roth[10] also showed that the Xe resonance lines at 1,470 and 1,296 Å had quite a different time history from that of the continuum in the visible. The visible continuum lasted for only 20 μsec while the resonance lines did not reach a maximum intensity until the continuum had nearly disappeared.

There have also been a number of studies of the spectral features of high temperature air. Of these, the most pertinent to the present investigation is that of Wood[12]. Wood analysed spectra obtained in the reflected shock region using a rapid-closing shutter. Considerable amount of molecular band radiation was observed. This was primarily from the N_2^+ (1st neg.) system at the lowest incident shock velocity of 6.4 km/sec. The band heads of the N_2 (2nd pos.) system also appeared but were considerably less pronounced. The line spectra due to the elements of O and N were in general prominent and narrow. However, at a speed of 8.29 km/sec the lines had become broad, the continuum had come up rapidly, and many lines were difficult to see above the continuum.

3. INSTRUMENTATION

Shock Tube

The shock tube used in this experiment is

one of the two arc-driven shock tubes available at the Ohio State University. The driven section is 10 cm in interior diameter, 8.5 meters long and made of stainless steel. The energy source of this facility is a capacitor bank with capacitance of 11,000 microfarads, which supplies the driver section with a maximum of 200,000 joules of energy at 6,000 volts. The discharge voltage can vary from 0 to 6,000 volts. The driver section is normally filled with helium at a pressure of 125 psig. A trigger wire in the driver section for initiation of the arc discharge extends through the wall and touches the inner anode. The main arc discharge is initiated by a discharge across the trigger wire. The arc heats the driver gas for about 80 μsec, thus causing an increase in the pressure in the driver. About 200–400 μsec after the initiation of trigger, the steel diaphragm prescored breaks into six pedals, and the heated gas travels into the driven section of the shock tube. Therefore, no radiation from the arc discharge propagates into the driven section. The recessed electrode in a "T" configuration also minimizes contamination of the driver gas.

A mechanical vacuum pump and a diffusion pump are connected in series close to the end wall of the driven section. Between the shock tube and the vacuum pump, a piston valve is installed. The valve makes the same contour as the inside surface of the shock tube when it is closed. The gas is evacuated to less than 2×10^{-4} torr. A thermocouple type pressure gage and CVC Phillips Cold Cathode Ionization Gage are used to measure the pressure in the driven tube during the evacuation and are also used to check leak rates. The leak rates are considered acceptable when they are less than 0.2×10^{-4} torr/min.

Synthetic air (21% O_2, 79% N_2) from Airco Industrial Gases and research grade xenon are used as test gases. In the case of both gases, to help minimize the contamination by room air, the shock tube was filled once with test gas and was evacuated again to less than 2×10^{-4} torr.

The test gas is once filled into a stainless steel tank of a known volume and then is released into the tube. The relation between tank pressure measured by a Wallace & Tiernen gage and the driven section pressure after the release was calibrated in advance using air. The Wallace & Tiernen gage is also

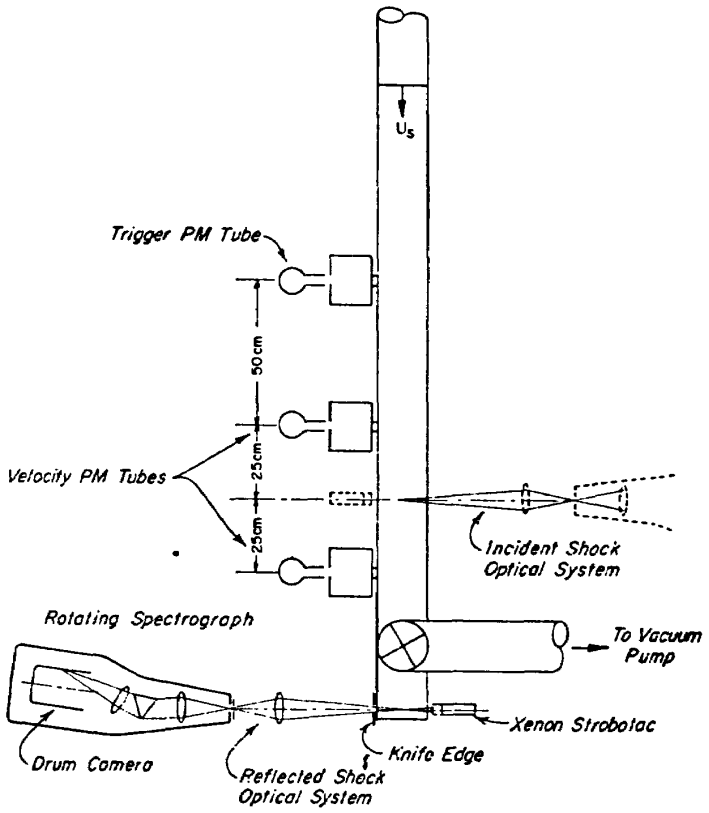

Figure 6. Schematic of OSU Arc-Driven Shock Tube and Optical System

calibrated with Macleod gage.

There are observation windows on the shock tube wall, as indicated in Figure 6. Six of them are used for this experiment in shock tube spectroscopy. Each window has a hole 22 mm in diameter and 5 mm in depth, which holds the 1 mm thick synthetic sapphire glass. Cut in the bottom surface of the hole is a slit with the dimensions of 1.5 mm in width and 14 mm in height. The first window with a phototube is used to monitor the passage of the shock front. The phototube is positioned at a distance 10 cm from the window. The second and fourth windows are located 50 cm apart, and the phototubes mounted at these two positions are used to measure the incident shock velocity. In front of each photomultiplier, there is a box with a collimation slit and neutral density filters. The slit allows only the beam from the window perpendicular to the shock tube axis to come into the photomultiplier. To decrease the brightness of the beam, the neutral plastic filter is changed to the one suitable for the photomultiplier. Utilizing the output of the first window with a certain time delay, the trigger signal is given to the oscilloscope monitoring the output of photomultipliers at the second and fourth windows.

Optical System

The spectrograph was coupled to the shock tube by the optical system as is shown in both Figures 6 and 7. This optical system was designed with two requirements in mind. First, the accepted beam had to cover the whole area of the collimator lens of the spectrograph to increase the resolving power of the spectra. Secondly, the solid angle of the light passing through the slit of the observation window and the focusing lens had to be small, so that the lens can see only a small distance in the axial direction. Consequently, this will decrease the overlapping time and increase the time resolution of the spectra. To satisfy both conditions, the lens must be positioned closer to the slit of the spectrograph than to the slit of the observation window. On the other hand, there is another condition that, in order to minimize the error of the distance from the slit of the spectrograph to the focusing point due to the error of the distance from the slit to the lens, the lens must be positioned in the middle of the distance between the slit and the focusing point. Therefore, the position of the lens must be settled compromizing those requirements. In the case of the incident shock wave observations, in order to increase the amount of light passing into the spectrograph, the lens is focused at 2.5 cm from the window inside the shock tube. The focusing lens is positioned halfway between the slit of the spectrograph and the center of the shock tube. The lens sees an area on the opposite wall, the side parallel to the tube axis being 4.5 mm and the side per-

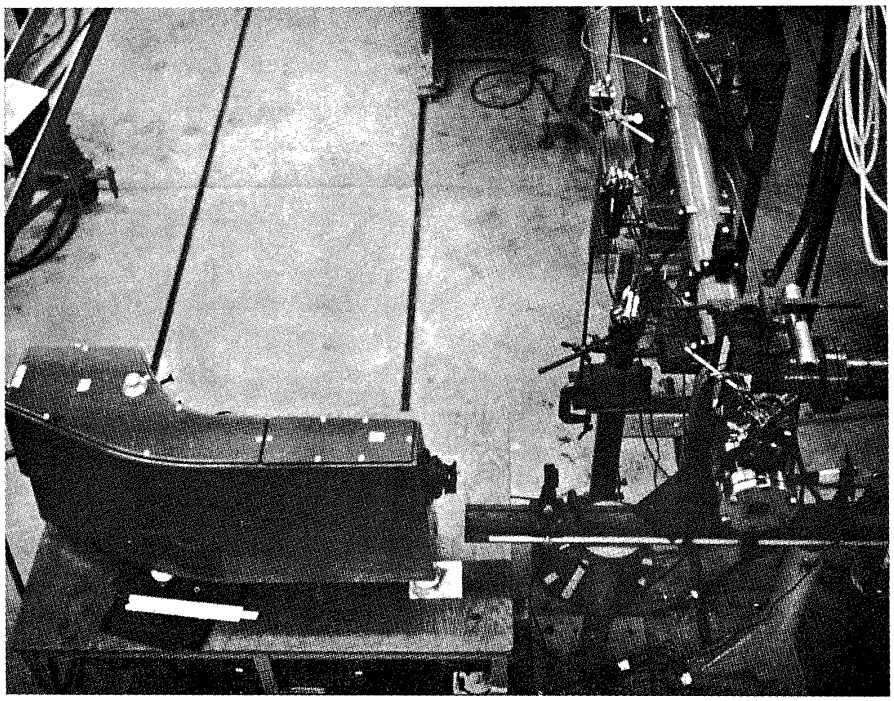

Figure 7. Photograph of Experimental Apparatus

pendicular to the tube axis being 5.5 mm. In the case of the reflected shock wave observations, the slits made of razor blades are set on the observation windows on both sides of the end wall. These slits are utilized to set the alignment of the optical system by a laser beam and to decrease the number of photons reaching on the film. The width of the slit is 1 mm. The center of the slit is positioned at 2.5 mm upstream of the end wall to avoid the light from the end wall coming into the spectrograph. The focusing lens was set closer to the slit of the spectrograph than to the window of the shock tube so as to increase the resolving power. In both cases, a Xenon Strobotac is flashed just before the arrival of the shock front. The image of the flash in the film is utilized to calibrate the shift of the reference line.

A B617 Large Aperture Spectrograph equipped with a rotating drum of the AVCO Rotating Drum Camera was used to take time-resolved spectra for both the incident and reflected shock waves. This spectrograph was designed specifically to produce a spectrum over the whole wavelength range from 2,000 to 10,000 Å. The slit aperture being large enough to allow short exposure times, this instrument is particularly suitable for the examination of the emission from transient discharges of short duration.

All the optical components are made from fused silica of excellent optical quality which is highly transmitting in the ultraviolet. The focal plane is flat and the emitted radiation may be recorded, for time resolution work, on a rotating drum camera. The optical components, i.e. bar, slit, collimator lens, prism, camera lens and plate holder of drum camera, are mounted on a base casting. The optical design of the instrument is as follows: the angle of the prism is 66°, the height 40 mm, and the face length 68 mm. The collimator lens has an aperture of 50 mm and a focal length of 559 mm at 2,500 Å. The front lens aperture of the camera is 58 mm, and the focal length at 2,500 Å is 151 mm. The relative aperture of the collimator is F/11, and that of the camera employed in connection with the prism is F/3.5. The wavelength range of the instrument is from 2,000 Å to 10,000 Å. The practical resolving power is from 3,000 to 10,000.

This instrument has several merits over the combination of a spectrograph with a rapid-closing, capping-type shutter. First of all, the said instrument can continuously record the change of radiation for more than 1,000 μsec. The changes of the radiation with respect to time can be recorded with an accuracy of approximately 1 μsec. However, the wavelength range covered on the 75 mm film is so large that identification of wavelength is more difficult than if a grating spectrograph is used.

The rotating drum of the AVCO Rotating Drum Camera, Type DC-060, MODEL 2, is used. The drum is a dynamically balanced cylinder, open at the front, bearing-mounted on a shaft supported between two ball seats. The drum is driven by the action of two compressed air streams directed against turbine buckets machined on the closed end of the drum. Usually, the drum is rotated by air at 70 psi with a speed close to 600 rps.

Before using the instrument in this study to take photographs of the time-resolved spectra behind incident and reflected shock waves, the best value of the tilt angle of the drum camera and the slit position were determined by taking spectra using pen-ray lamps. Setting the mercury and neon pen-ray lamps in front of the slit of the spectrograph alternately and focusing the beam with a quartz lens on the slit, the spectra were exposed on the interior of the drum. The drum was rotated about 2 cm for every exposure by hand. The slit was moved from 3.0 to 6.0 mm at the interval of 0.5 mm for one tilt angle of the drum. The angle was changed from 3.0° to 5.5° at intervals of 0.5°. Those spectra were then compared in terms of focusing. A 4.25° drum tilt angle and a 3.75 mm slit position gave the best focusing effect. The adjusted position was maintained throughout all the experiments.

Recording Film

Kodak TRI-X and Kodak 2475 Recording Film were used. The latter is an extremely highspeed panchromatic film (ASA 1000) with extended red sensitivity up to 7,000 Å. It is especially effective in recording the incident shock spectra of air, for which purpose Kodak TRI-X is not adequate to produce satisfactory images. After each shock tube test, the reference lines using a mercury pen-ray is exposed on the film. The duration of this exposure was changed depending on the developing time of the film. It was developed for different durations in room-temperature HC-110, even if the duration exceeded the developing time recommended by the manufacturer. For incident shock waves in air, it was developed for more than twelve minutes. For xenon, it was de-

veloped for ten minutes to get the whole incident shock image, and three minutes to get the details of the bright region on the image. In the latter case, the weaker image almost faded away. Due to different periods of developing used to suit different conditions of the film, it was not possible to determine the amount of light exposed on a given film on the basis of the brightness thereof. This permits qualitative comparisons of lights exposed only on the same film. Unfortunately, the high speed film is grainy and the 2475 film is rated coarse-grained. This reduces the resolving power and increases the noise level when it is scanned by microdensitometer with a fixed slit height.

Microdensitometer

A Jarrell-Ash 21-000 Microphotometer is used to scan the spectra on a film. The spectra on a film may be hand-scanned or moved across the slit at a constant speed of 6, 12 or 18 microns per second by a motor drive. As the photographic film is scanned slowly across the aluminum mirror, the images of the spectral lines move across the slit. The light detected by the photomultiplier is that transmitted by the line image. For the 10.0% change of power supply voltage, the output reading does not change appreciably. The drift of the output is less than plus or minus 3% for a period of one hour or more. The height of the slit is changeable step-wise, while the width can be increased continuously. There is also a knob to set the slit parallel to the spectra. The output of the photomultiplier is recorded by the potentiometertype chart recorder. The chart speed may be controlled by replacing the gear of the chart drive.

Identification of Spectra

To identify the spectra, the film was scanned at the speed of 1.5 mm/min by microdensitometer, and recorded by the potentiometer-type recorder, the chart of which moves 5 in/min. The width of the microdensitometer's slit is set at 7 μ and the height is selected from between 0.5 and 2.0 mm. Where the darkness of spectra on the film changes rapidly in the time direction, the height of 0.5 mm is used at the cost of accuracy, and where the darkness changes slowly, the height of 2.0 mm is used to reduce the noise.

To identify the spectra, the Hartmann dispersion formula is used. This greatly reduces the number of reference lines. For wavelength calculation, the equation is as follows:

$$\lambda=\lambda_0+\frac{c}{d_0-d}$$

where λ_0, c and d_0 are constants. This expression represents the dispersion curve of a spectrograph with a satisfactory degree of approximation. For the determination of the three constants of the Hartmann formula λ_0, c and h, the reading of three reference lines are needed. Several forms have been given for the solution of the three simultaneous equations resulting from the substitution of the three pairs of values in the formula. The form found convenient at the University of Michigan for machine calculation was employed here[13] with an accuracy in the region of 2536–5460 Å of about 1 Å. Reference 14 was used to identify the spectral lines.

4. RESULTS AND DISCUSSIONS

Incident Shock Wave Spectra in Air

Figure 8 shows the spectral photograph obtained in air at $P_1=1.0$ torr and $U_S=10$ km/sec. In order to define the wavelength, the film was exposed to a mercury pen-ray lamp for 15 seconds immediately following the test and resulting reference lines are indicated by wavelength in Figure 8. The photograph shows an extremely grainy image since it was developed for 13 minutes (five times the recommended developing time of the manufacturer). However, it was possible to obtain some qualitative results from such spectra.

The photograph clearly illustrates the contact surface between the incident shock-heated test gas and the driver gas. This contact surface is followed by a bright spectra which is actually the contact region containing air mixed with helium. This bright spectra is different from that observed in xenon where the test gas is not followed by a region exhibiting a bright spectra. This phenomenon appears to be largely due to the effect of iron, and may suggest the existence of chemical reactions between iron and air. The intensity of this region is certainly governed by the cooling associated with the expanding driver gas flow. The spectra from the incident shock wave region also extends into this region. Unlike the case of xenon, the intensity of the spectra in the incident shock region for air does not exhibit radical time changes, but gradually reduces in strength from the middle of the test region and on back. This fact is evident from the total radiation photomultiplier records which were obtained, but are not shown here.

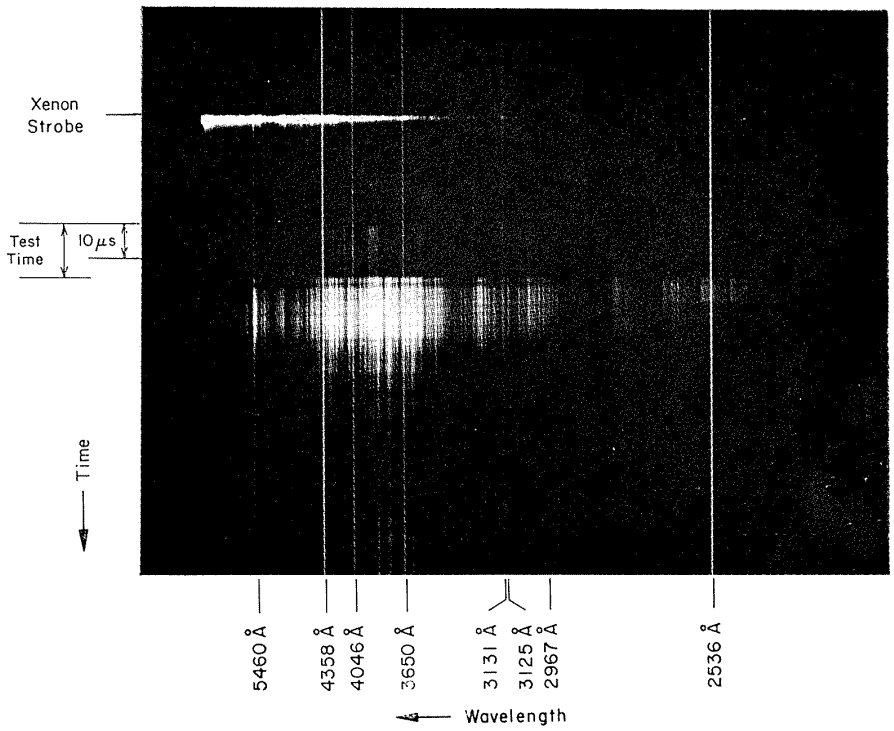

Figure 8. Time-Resolved Spectrogram Behind Incident Shock Wave in Air; $p_1=1.0$ torr, $U_s=10.0$ km/sec.

In some experiments, however, spectra very similar to that observed to occur following the contact surface appear (somewhat suddenly) in the latter half of the test time, and are followed by the restoration of the normal test region spectra.

The test region of the spectral photographs have been scanned and a typical result is shown in Figure 9. In order to reduce the noise level, the microdensitometer slit was set at 7 μ in width and 2 mm in length. The figure shows the $(n+1, n)$ and (n, n) bands of N^+_2 (1st negative). Although the $(n, n+1)$ band exists, the band head is not clear. The transitions marked R are reference lines. The figure also indicates the existence of what looks like the spectrum of OI, but it cannot be determined. The close existence of the spectrum of FeII and coarse grains in the film bothered the identification of the spectrum. The distribution of the spectrum bears a close resemblance to that of the spectrum observed by Wood behind a reflected shock wave at $U_S=6.40$ km/sec and $P_1=0.2$ torr[12].

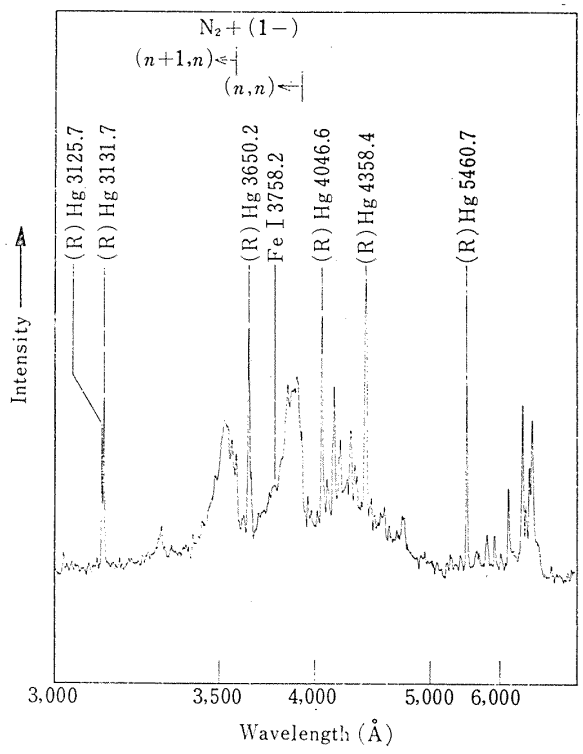

Figure 9. Microdensitometer Trace of Test Gas Region of Spectrogram Obtained Behind Incident Shock Wave in Air; $p_1=1.0$ torr, $U_s=10.0$ km/sec.

Incident Shock Wave Spectra in Xenon

Experiments were made at both $P_1=0.1$ torr and 1.0 torr and with the bank voltage for the arc-driven shock tube set from 28,000 to 6,000 V. Figure 10 shows a spectral photo-

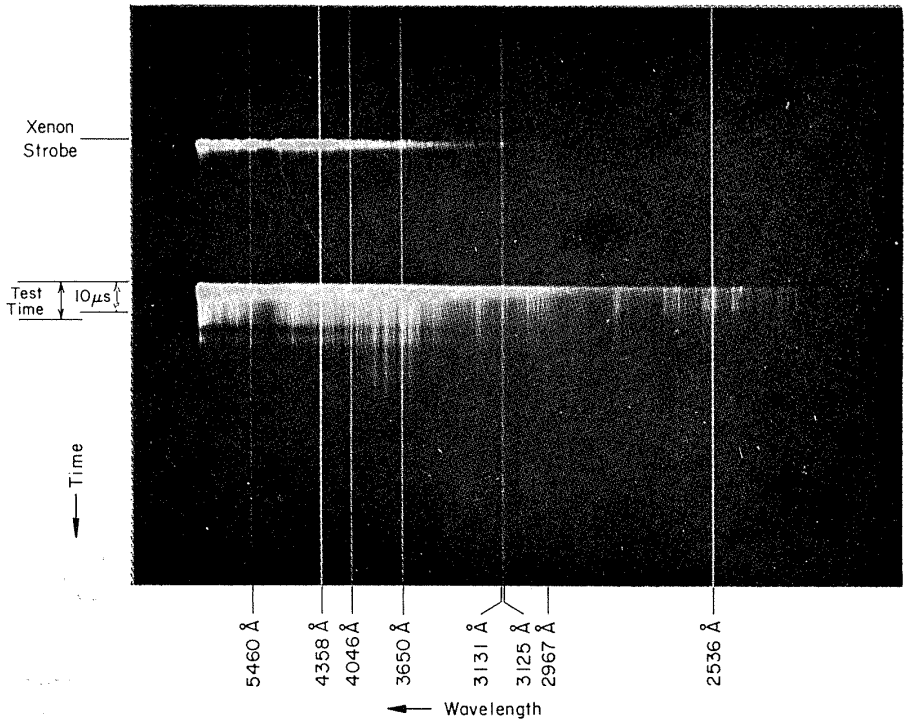

Figure 10. Time-Resolved Spectrogram Behind Incident Shock Wave in Xenon, $p_1=1.0$ torr, $U_s=4.5$ km/sec.

graph taken at $P_1=1.0$ torr and for $U_S=4.5$ km/sec in xenon. For about 3 μsec, the spectra demonstrates an extremely bright intensity and shows the existence of a strong continuum. The phenomenon is more prominent at $P_1=1.0$ torr than at $P_1=0.1$ torr. The line spectra has a distribution even below 2,500 Å.

It becomes evident by reducing the developing time of the film for a given experimental condition that a strong line spectra is also resident, overlapping with the continuum. In this instance, however, the weaker spectra in the latter portion of the test region become eliminated.

Within the shock wave range of 4–7.5 km/sec, and especially in the case of $P_1=1.0$ torr, the observed spectra show within a few μsec after passage of the shock front, in many cases, a strengthening of the intensity, followed by an immediate weakening and then a strengthening again. This is accompanied by the strengthening of the continuum. The cause for this double structure has not been determined.

Figure 11 shows the scanning of the test gas region of the shock-heated gas for a test similar to that of Figure 10. The slit width was set at 7 μ and the slit height at 0.5 mm. It is inferred from this figure that strong XeII line transitions exist in the 5,000–3,500 Å wavelength region, but they decline rapidly in intensity after a few μ seconds. XeII and XeIII lines exist in the ultraviolet region, however, FeI and FeII lines lie at almost the same position and it is difficult to distinguish the XeII and iron lines from each other.

FeI and II appear to have existed almost from the start of the test time. This is believed to be due to radiation from contamination within the boundary layer, presumably originating on the shock tube wall.

Additional scans of incident shock wave spectra in xenon are shown in Figures 12 and 13. These are for a pressure of 0.1 torr, however, it is not possible to make quantitative comparisons between these. The existence of a particularly large number of sharp lines in Figure 12 and 13 (these in general are unmarked) is explained by the presence of strong FeI and FeII radiation. It is also accounted for by the increased continuum intensities at $P_1=1.0$ torr which suppresses these lines.

Reflected Shock Wave Spectra in Air

The radiation behind reflected shock waves has been observed over a range of incident shock speeds in air and for $P_1=1.0$ torr. The observation window used in these measurements is at the side of the end wall, has a slit

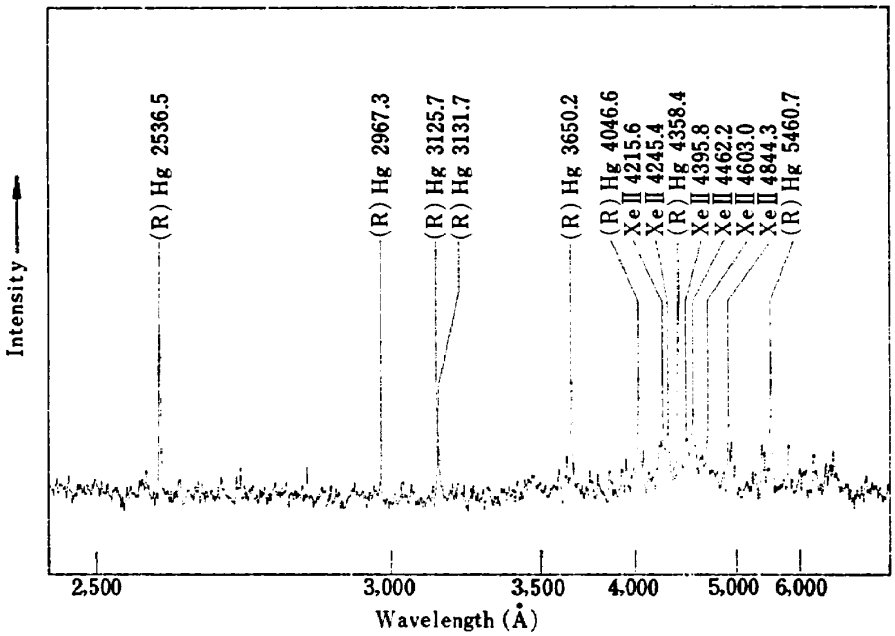

Figure 11. Microdensitometer Trace of Test Gas Region of Spectrogram Obtained Behind Incident Shock Wave in Xenon; p_1=1.0 rorr, U_s=4.0 km/sec.

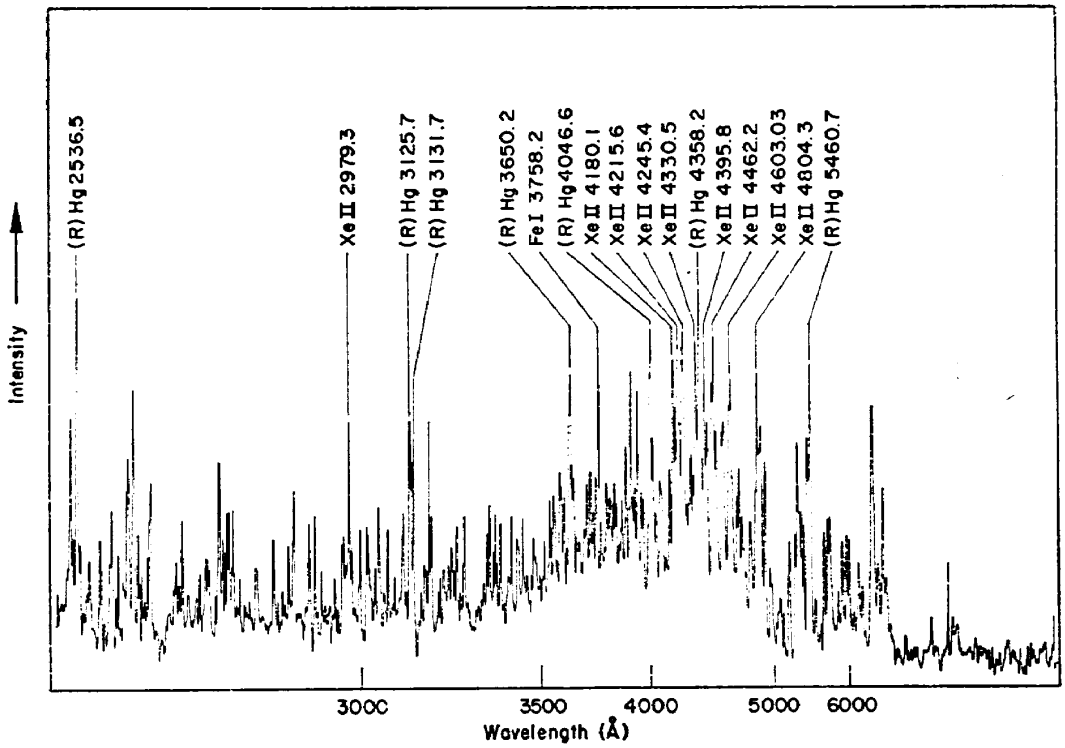

Figure 12. Microdensitometer Trace of Test Gas Region of Spectrogram Obtained Behind Incident Shock Wave in Xenon; p_1=0.1 torr, U_s=7.47 km/sec.

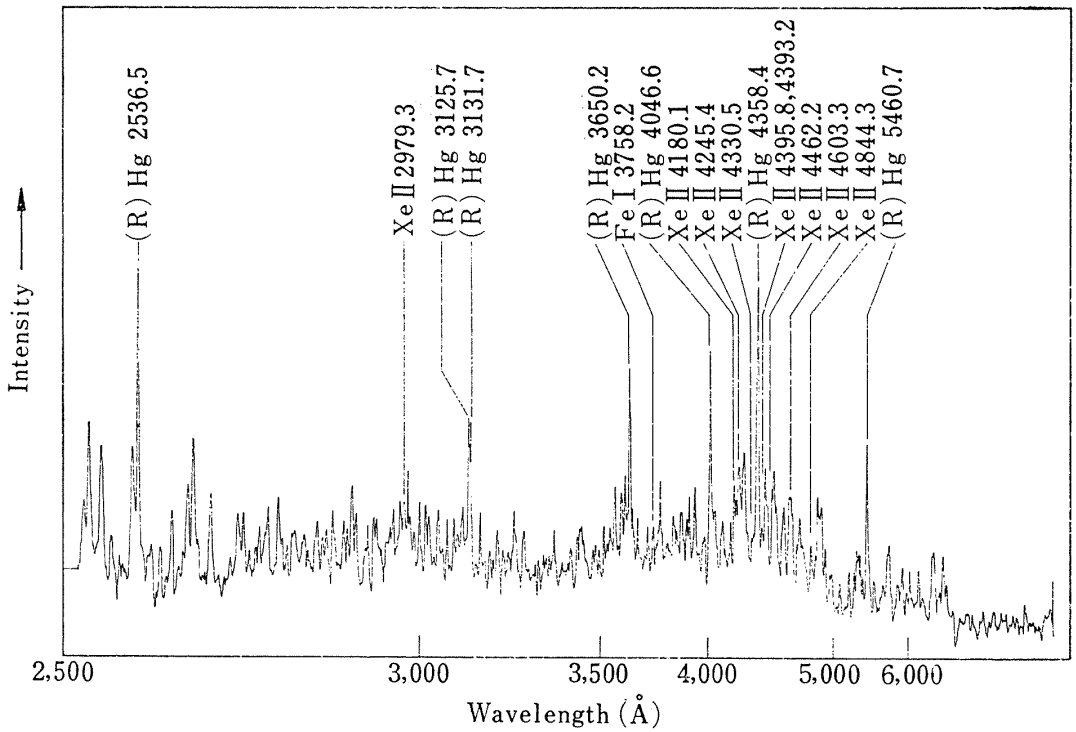

Figure 13. Microdensitometer Trace of Test Gas Region of Specrogram Obtained Behind Incident Shock Wave in Xenon; $p_1=0.1$ torr, $U_s=9.27$ km/sec.

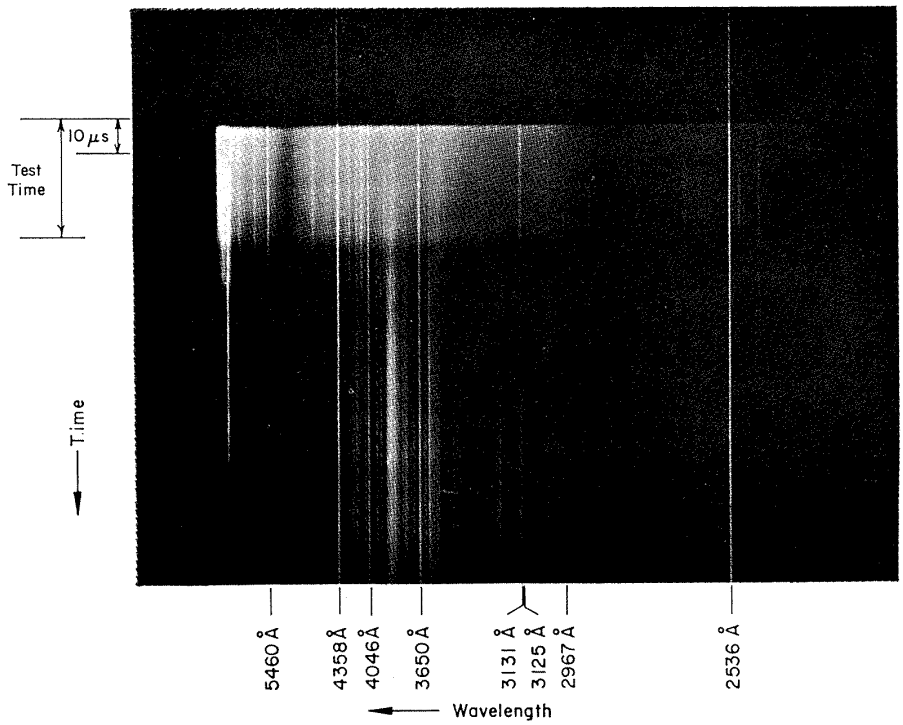

Figure 14. Time-Resolved Spectrogram Behind Reflected Shock Wave in Air; $p_1=1.0$ torr, $U_s=9.6$ km/sec.

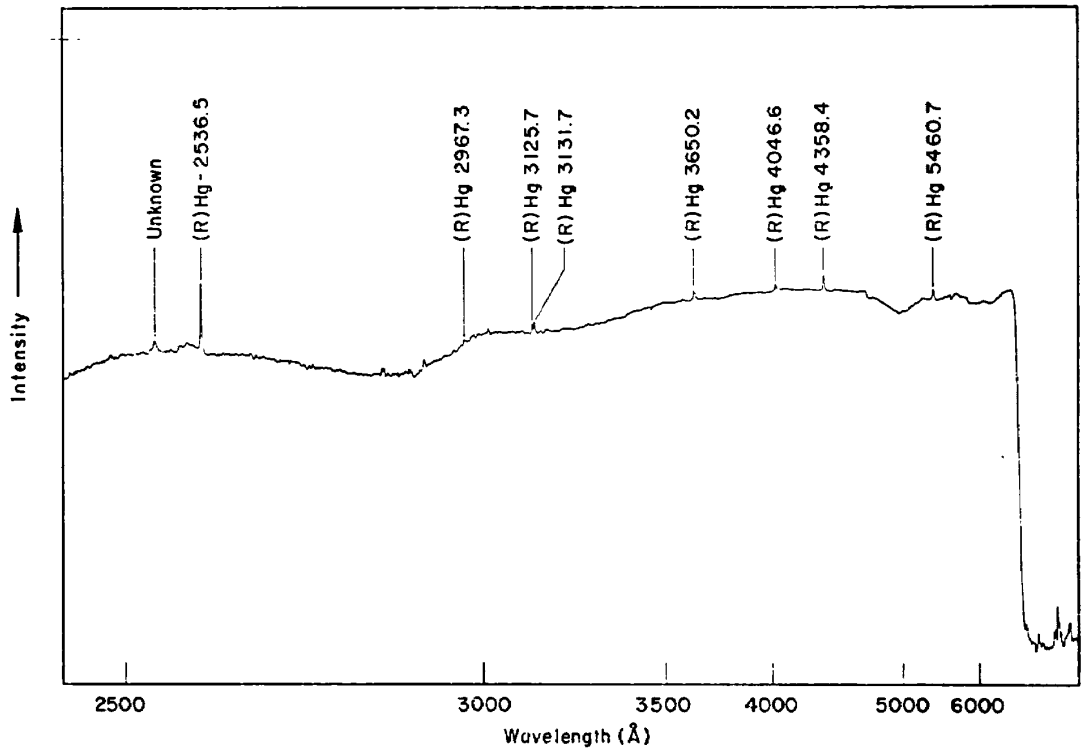

Figure 15. Microdensitometer Trace of Test Gas Region of Spectrogram Obtained Behind Reflected Shock Wave in Air; $p_1=1.0$ torr, $U_s=9.6$ km/sec.

1.0 mm wide, and the center of its position is 2.5 mm upstream from the end wall. The incident shock speed ranged from 7.4 to 9.63 km/sec. One of the cases for which spectra was observed is shown in Figure 14. For this case $U_S=9.6$ km/sec. As may be seen, it is not easy to determine the end of the test time on this spectral photograph of radiation from the reflected region because near the end wall the contact surface does not pass by the observation window. The time resolved spectra from the reflected shock region does show us, however, the change in properties of the shock-heated air with time. In that portion of the photograph in Figure 14 which corresponds to the test region, the film exposure is dominated by the continuum. Gradually absorption lines of FeI and FeII appear on the continuum spectra near the end of the test time and the continuum spectra begins to fade away, starting first in the ultraviolet region.

For the case of $U_S=7.14$ km/sec (not shown here), the demarcation of the continuum is clearer than in the higher speed case. After the test time the continuum rapidly begins to fade and the spectra of FeI and FeII become clear. The trace scanned by the microdensitometer close to the beginning of the test region in Figure 14 is shown in Figure 15. There are many lines in the continuum but the continuum is so bright that the densitometer cannot pick up these lines distinctly. The trace scanned just after the end of the test time showed that in the continuum there are many spectral lines of FeI and FeII appearing in emission. This fact is quite opposite to that found at the higher shock velocities where some iron lines are observed to appear in absorption. The trace scanned about 70 μsec after shock passage shows that the band heads of N_2^+ (1st negative) begin to appear and the trace looks very similar to that of incident shock wave spectra in air if we ignore the presence of the iron lines.

Reflected Shock Wave Spectra in Xenon

A spectral photograph of the reflected shock-heated region in xenon was filmed at $P_1=1.0$ torr and $U_S=5.9$ km/sec. The photograph shows the spectra of the incident shock wave for a time period of about 2 μsec prior to the arrival of the reflected shock front when the spectra of the reflected shock-heated gas appears. The spectra from the reflected shock region indicate the existence of a strong absorption of the spectra resulting from the iron

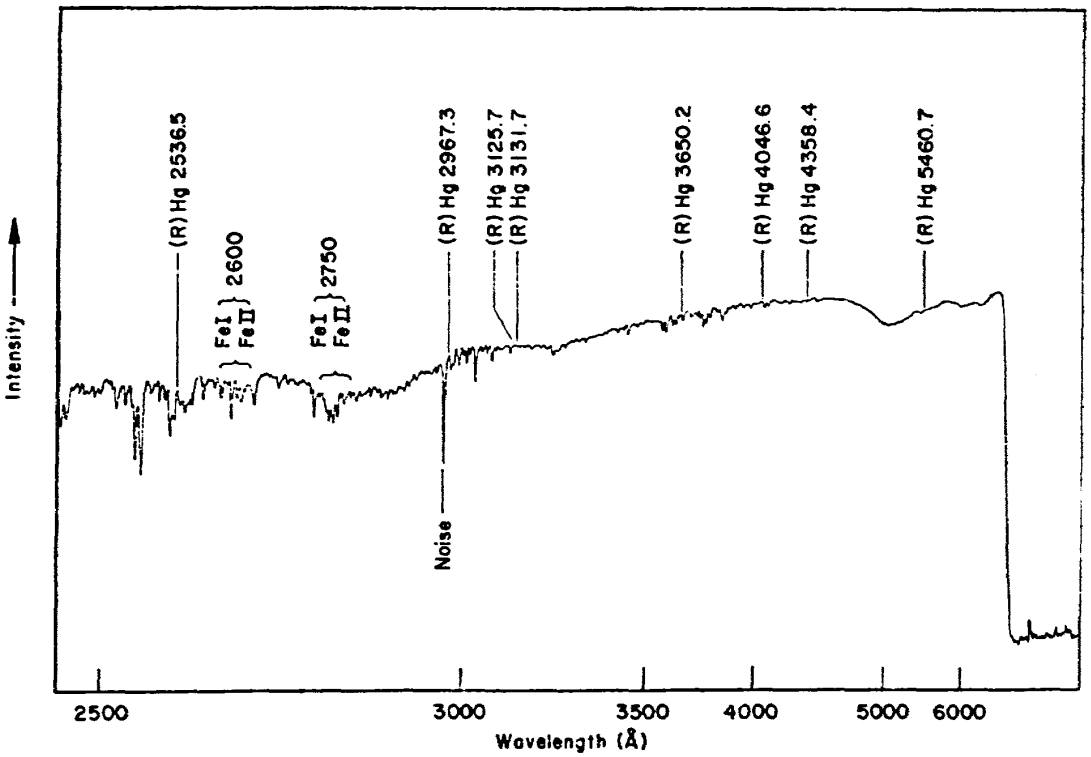

Figure 16. Microdensitometer Trace of Test Gas Region of Spectrogram Obtained Behind Reflected Shock Wave in Xenon, p_1=1.0 torr, U_s=5.88 km/sec.

lines. The brightness of the spectra is especially strong at 1–2 μsec after passage of the reflected shock front, followed by about 10 μsec of a region steady in intensity, and this is considered the test time of the reflected shock wave region. The spectra subsequently alternates in strength with a regular interval before diminishing from the ultraviolet side. Figure 16 demonstrates the result obtained from scanning the test region of the reflected shock wape spectra, and indicates the strong absorption due to iron in the continuum spectra. The decrease in the strength on the ultraviolet side and in the neighborhood of 5,200 Å is explained by the dual effects of the film sensitivity and the behavior of the continuum radiation, and therefore it is difficult to learn anything about the intensity distribution of the continuum spectra from this measurement.

Test Time

Due to the effects of the boundary layer, i.e. the loss of mass to the contact region, the actual test time in a shock tube is considerably less than that predicted by ideal theory. In order to assess the available test time for the conditions of the present experiments, estimates of test time have been obtained from the time-resolved spectra and compared with photomultiplier measurements of the post-incident shock radiation luminosity time-history. The two photomultipliers employed in this latter measurement were located 25 cm upstream and 25 cm downstream of the observation window used in obtaining the incident shock wave spectra. These photomultipliers recorded the output of the integrated radiation from the window through a slit system. For incident shock waves in air, it is easy to determine the test time. The averaged value of the two test times obtained with the photomultipliers was found to agree well with the value defined by the time-resolved spectra within an error of about 1–2 μsec. For example, at incident shock velocities of 9.8 and 10.0 km/sec, the respective test times obtained from the time-resolved spectra were 20.0 and 14.3 microseconds. The corresponding values obtained from the photomultiplier measurements were 19.5 and 15.0 microseconds.

For the case of xenon, definition of the test time is accompanied by greater error, because the radiation decreases rapidly after the shock front, and the oscilloscope output is quite low

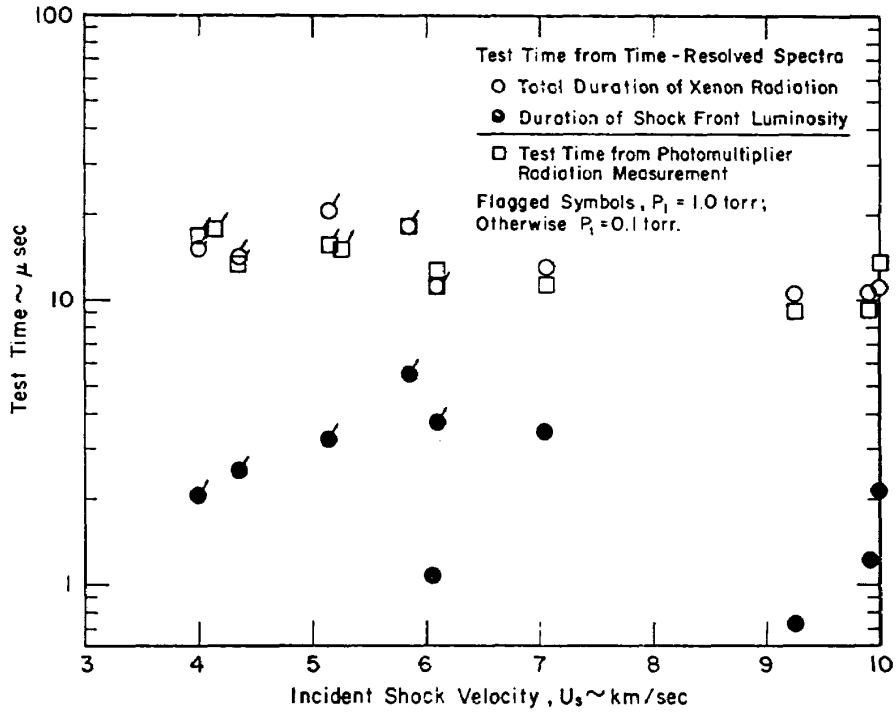

Figure 17. Test Time Measured Behind Incident Shock Wave in Xenon, p_1=0.1 torr and 1.0 torr

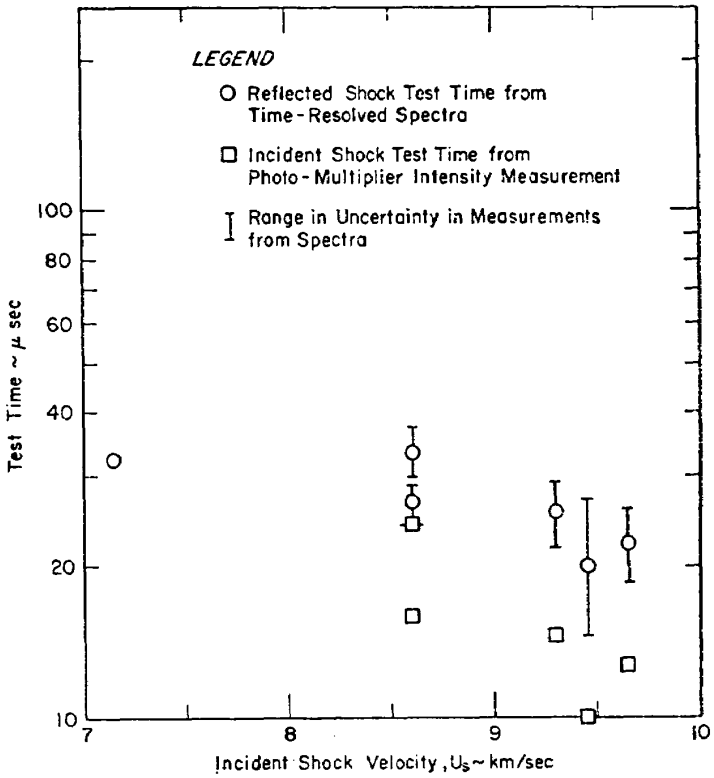

Figure 18. Comparison of Measured Test Times Behind Incident and Reflected Shock Waves in Air, p_1=1.0 torr.

at the end of the test time. In the case of the reflected shock waves, there is again similar trouble in defining the end of test gas region.

In Figure 17, the incident shock wave test time for xenon as observed both with the photomultiplier and by the time-resolved spectra is shown. As may be seen, there are two values for the test time measurements from the spectra which are indicated. The one is in reasonable agreement with the value indicated from the broad band photomultiplier measurements. The other is considerably less; however, it is in better agreement with earlier results obtained at the Ohio State University[16]. This latter region is associated with the major luminosity portion of the test gas. It is believed that after this region the xenon, though still strongly radiating, becomes partially quenched by mixing with the helium in the contact region. Thus the smaller value is the actual test time.

Measurements of available test time in the reflected shock region in both air and xenon have also been carried out. If the test time of the reflected shock region is defined as the time between the reflection of the incident shock wave at the end wall and the collision of the reflected shock front with the contact surface, then normally the incident shock wave test time will be slightly greater than this reflected shock test time. In this experiment the measured reflected shock test time is the real test time observed at a point 2.5 mm upstream of the end wall, and in Figure 18 these measurements are compared with the incident shock wave test time measured with a photomultiplier on the same test 2 feet further upstream. As may be seen, the reflected shock test time is on the order of twice the corresponding incident shock test time. This is because after the reflected shock wave collides with the contact surface, there is a finite amount of time before the effect of this propogates back to the end wall.

A single measurement of the reflected shock test time was made in xenon using the time-resolved spectra. This yielded a value of 10 microseconds at a shock velocity of 5.88 km/sec in xenon at a pressure of 1.0 torr.

5. CONCLUSIONS

Time-resolved spectra have been obtained behind incident and reflected shock waves in air and xenon at initial pressures of 0.1 and 1.0 torr using a rotating drum spectrograph and the OSU arc-driven shock tube. These spectra were used to determine the qualitative nature of the flow as well as for making estimates of the available test time.

The $(n+1, n)$ and (n, n) band spectra of N_2^+ (1st negative) were observed in the test gas behind incident shock waves in air at $p_1=$ 1.0 torr and $U_S=9$–10 km/sec. Behind reflected shock waves in air, the continuum of spectra appeared to cover almost the entire wavelength of 2,500–7,000 Å for the shock-heated test gas.

For xenon, the spectra for the incident shock wave cases for $p_1=0.1$ torr show an interesting structure in which two intensely bright regions are witnessed in the time direction. This phenomenon was distinct at high pressure and low velocities, but was not seen at the higher velocities, for example at $p_1=0.1$ torr and $U_S=9$–10 km/sec. To understand these phenomena, extensive experiments are necessary. The spectra obtained behind reflected shock waves in xenon was also dominated by continuum radiation but included strong absorption spectra due to FeI and FeII from the moment the reflected shock passed and on.

In most cases, the spectra due to FeI and FeII were observed in the test time and this is most likely due to contamination in the boundary layer.

The test time measurements obtained behind incident shock waves in xenon using both the photomultiplier outputs and the spectra were in reasonable agreement, although the interpretation of the spectra was somewhat open to question. Test time measurements using the time-resolved spectra were also carried out behind the reflected shock waves.

ACKNOWLEDGMENT

This work was done in the Department of Aeronautical and Astronautical Engineering at the Ohio State University.

The author wishes to thank here the organizations and the individuals who have made major contributions to the completion of this work. My sincere thanks go to the National Aeronautics and Space Administration and the Air Force Office of Scientific Research which provided financial support for this work through Grant No. NGR-36-008-163 and Grant No. AFOSR-69-1759.

The author wishes to thank Mr. Jon B. Bader, Mr. Jonathan Dann and Mr. Micheal Culp for their devoted assistance and constructive criticisms throughout the course of this experimental investigation, especially for making avail-

able the equipment used in the experimental work.

And finally the author also wishes to thank his adviser, Dr. Robert M. Nerem, whose constant assistance and guidance greatly aided the completion of this work.

REFERENCES

1) Golobic, Robert A.: A Laboratory Study of Strong Shock Waves in Xenon, Ph.D. Dissertation, Department of Aeronautical and Astronautical Engineering, The Ohio State University, 1971.
2) Bader, Jon B.: The Development of a Brightness Temperature Measurement Technique for Application to Shock-Tube Produced Flows, Master Thesis, Department of Aeronautical and Astronautical Engineering, The Ohio State University, 1971.
3) Crawford, Keith E.: A Method of Calculating Equilibrium States Behind Incident and Reflected Shock Waves in Ionizing Monatomic Gases, Master Thesis, Department of Aeronautical and Astronautical Engineering, The Ohio State University, 1969.
4) Menard, W. A. and Horton, P. E.: Shock-tube Thermal Chemistry Table for High-temperature Gases; Air, Jet Propulsion Laboratory Technical Paper 32–1408, Vol. I 1969.
5) Gaydon, A. G. and Hurle, I. R.: The Shock Tube in High-Temperature Chemical Physics, Reinhold Publ., New York, 1963.
6) Herzberg, G.: Atomic Spectra and Atomic Structure, Dover Publ., New York, 1950.
7) Herzberg, G.: Molecular Spectra and Molecular Structure, I. Diatomic Molecules, Van Nostrand, New York, 1950.
8) Penner, S. S.: Quantative Molecular Spectroscopy and Gas Emissivities, Addison-Wesley, New York, 1959.
9) Zel'dovich, Ya. B. and Raizer, Yu. B.: Physics of Shock Waves and High-Temperature Hydrodynamic Phenomena (Vol. 1), Academic Press, New York, 1966.
10) Roth, W. J.: Chem. Phys., 32, p. 1876, 1960.
11) Gloersen, P.: Phys. of Fluids, 3 p. 857, 1960.
12) Wood, Allen D.: Radiant Energy Transfer Measurements in Air, NASA CR-1390, 1969.
13) Sawyer, R. A.: Experimental Spectroscopy, Dover Publ. Inc., New York, 1963.
14) Striganov, A. R. and Sventiskii, N. S.: Tables of Spectral Lines of Neutral and Ionized Atoms, IFI-Plenum New York, 1968.
15) Smith, J. J.: An Initial Study of Shock-Heated Xenon Using an Arc-driven Shock Tube, Master Thesis, Dept. of Aeronautical and Astronautical Engineering, The Ohio State University, 1970.

TR-348	Effect of Atmosphere on Boundary Lubrication (I)	Makoto NISHIMURA	Sept. 1973
TR-349			
TR-350	Dynamic Responses of the Structure Model with Built-Up Wings and a Fuselage (I)	Taketoshi HANAWA & Keiji KOMATSU	Dec. 1973

TECHNICAL REPORT OF NATIONAL AEROSPACE LABORATORY
TR-351T

航空宇宙技術研究所報告 351T号 (欧文)

昭和 48 年 12 月 発行

発行所 航空宇宙技術研究所
東京都調布市深大寺町 1,880
電話 武蔵野三鷹 (0422)47-5911 (大代表)

印刷所 株式会社 東京プレス
東京都板橋区桜川 2 丁目 27 の 12

Published by
NATIONAL AEROSPACE LABORATORY
1,880 Jindaiji, Chōfu, Tokyo
JAPAN

Printed in Japan